

# A Novel RF Ranging Method

Ákos Lédeczi, Péter Völgyesi, János Sallai, Ryan Thibodeaux  
Institute for Software Integrated Systems,  
Vanderbilt University, Nashville, TN, USA  
akos.ledeczi@vanderbilt.edu

## Abstract

*Localization and tracking of wireless nodes have been active research areas in robotics, mobile ad-hoc networks, and wireless sensor networks. While several phenomena have been utilized for this purpose, RF signals have many advantages. Signal strength and time-of-flight are the two typical ways of extracting range information. Recently, radio interferometry was proposed to solve this problem using phase and/or Doppler shift measurements across severely resource-constrained devices. The former requires many measurements at multiple frequencies, while the latter needs motion to generate a usable signal. This paper introduces a novel ranging method based on a rotating antenna generating a Doppler shifted RF signal. The frequency change can be measured using the radio interferometric technique even on low-cost, resource constrained devices. This simple idea provides a surprising number of different ways for estimating range and location. The paper outlines these techniques and describes one of them in more detail with experimental and simulation results.<sup>1</sup>*

## 1: Introduction

Mobile ad-hoc networks (MANET), wireless sensor networks (WSN) and unattended air or ground vehicles (UAV, UGV) are prime examples where location-awareness is a key requirement. While there are many practical localization systems, there are still applications with such requirements that none of the existing solutions is satisfactory. The most popular localization method is GPS, for example, but it typically does not work indoors and its price and power requirements prohibit its use when low cost and/or very long lifetime are the main design drivers. Techniques based on ultrasonic and infrared signal modalities have short range and require line-of-sight. Clearly, RF-based approaches hold the most promise for many reasons. A radio is already available on any wireless node, so it comes at no added cost and it is already included in the power budget. RF range is superior to most other signals. Line-of-sight may not be necessary, since radio signals may propagate through walls; however, radio propagation, especially indoors, presents significant problems of its own.

Radio signal strength (RSS)-based approaches are the most straightforward for estimating distance from an RF signal; however, such methodologies are relatively imprecise due to fading. The accuracy of numerous RSS techniques is typically meter-scale [2][15]. The Location Engine [13] developed at Motorola Research depends on RSS measurements and

---

<sup>1</sup>This work was supported in part by NSF grant CNS-0721604 and ARO MURI grant W911NF-06-1-0076.

anchor nodes at known positions. Chipcon (now Texas Instruments) licensed and integrated the technology into the CC2431 transceiver chip and claims 3 m accuracy. Active RFID systems use self-powered tags to identify and locate objects. For example, PanGo is a commercial asset tracking system using 802.11 active RFID tags [11] providing room-level resolution relying on dense access point infrastructure.

Recently, a radio interferometric solution was proposed for the localization and tracking of resource-constrained wireless nodes [10][8]. By measuring the phase difference of a signal generated by two transmitters with close frequencies at two receivers, information on the relative distances of the four nodes involved can be deduced. While both the range and the accuracy of the method proved superior to many other approaches [7][14], multipath propagation impacts the accuracy of the method. Also, the ranging needs to be carried out at multiple frequencies which can be time consuming. A variation of the method replaces the phase measurements with that of frequency. The technique assumes a moving transmitter at an unknown location (and with an unknown velocity vector). As such, it generates a Doppler shift. If this shift is measured at multiple receivers, the location and velocity of the tag can be accurately estimated [9]. The reference implementation works on Crossbow Mica2 nodes operating at 430 MHz [3]. A person walking with the transmitter at 0.3 m/s induces a 0.4 Hz shift, a  $10^9:1$  ratio, which is impossible to measure directly on the cc1000 radio chip or on much more expensive instrumentation either. However, if a second, stationary node transmits a radio signal a few hundred Hz away from the moving node's frequency, the envelop signal (measured as the RSS of the composite signal) has a few hundred Hz frequency. The Doppler shift also appears in this signal and can be measured accurately enough using simple, inexpensive hardware.

The obvious disadvantage of this method is the requirement for movement, since without it, there would be no Doppler shift. This observation lead us to the idea of rotating the antenna of the transmitter (or even the entire node) at a constant speed and radius. To a stationary observer, the signal will have a continuously changing frequency. Again, radio interferometry is required to be able to measure this accurately. How the frequency changes over time depends on the angular velocity of the transmitter, the radius of the circle, and the distance between the rotating transmitter and the receiver. While it is straightforward to compute the distance given the Doppler shift, the radius and the angular velocity, the result is very sensitive to measurement errors if the distance is large. To tackle this issue, we leverage the fact that the correlation of the observed frequency change across multiple receivers provides valuable information on the location of the nodes involved.

The remainder of the paper describes the ranging approach in more detail, the hardware setup and the signal processing algorithms used for experimentation, followed by experimental and simulation results. We have only taken our initial steps in this promising direction, so we conclude the paper with future research directions.

## 2: Ranging approaches

Rotating a radio transmitter results in a continuously changing frequency at a stationary observer due to the Doppler Effect. The amount of the Doppler shift depends on the transmit frequency and the instantaneous relative velocity of the two nodes. Consider Figure 1(a) where transmitter  $T$  rotates at a constant angular rate ( $\omega$ ) and radius ( $r$ ) and receiver  $R$  measures the frequency of the signal. The maximum of the frequency is observed

at point  $A$  where the transmitter moves directly toward the receiver, while the minimum frequency is measured when the transmitter is at point  $B$  moving exactly away from the receiver. Figure 1(b) shows the observed frequency at the receiver when it is 10 meters away from the transmitter rotating with 12 cm radius at 45 revolutions per minute (RPM) and transmitting at 430 MHz.

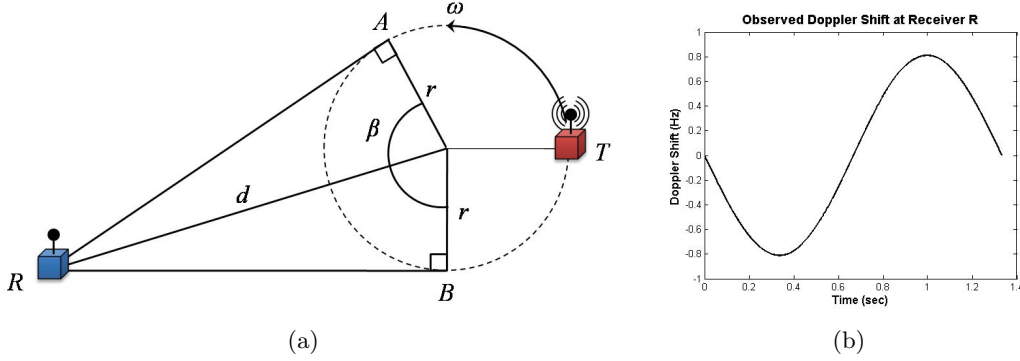


**Figure 1. (a) Range estimation method (b) Range estimation results**

The maximum of the observed Doppler shift is approximately  $\pm 0.8$  Hz. Directly measuring frequency with that kind of accuracy would be challenging even with expensive laboratory instruments. However, by introducing an arbitrarily positioned second transmitter ( $T'$ ) and tuning the two transmitter frequencies such that  $T'$  is transmitting at a slightly lower frequency than  $T$  (for example, at 1 kHz or less), the envelope of the signal observed at a receiver will have a frequency corresponding to this difference [10]. Consequently, the Doppler shift due to the rotation of one of transmitters causes the same amount of Doppler shift in the envelop signal. This can be measured accurately even with low cost equipment. Furthermore, the location of the stationary transmitter has no effect on the observed frequency.

Consider Figure 1(a) again. By measuring the time between the two extrema of the frequency shift, the angle  $\beta$  can be estimated given the angular speed of the transmitter. Hence, the range between two nodes can be estimated this way. However, it is easy to show that this method is very sensitive to measurement noise when the distance between the transmitter and the receiver is large compared to the radius of rotation. However, introducing a second receiver offers another method for ranging.

Both receivers  $R_1$  and  $R_2$  in Figure 2(a) continuously measure the frequency of the beat signal. Let us denote the velocity vectors of  $R_1$  and  $R_2$  relative to the velocity vector of the rotating transmitter as  $\vec{v}_1$  and  $\vec{v}_2$ , respectively. Vectors  $\vec{v}_1$  and  $\vec{v}_2$  are obviously related. From the observed magnitude of both vectors at the point of the maximum frequency shift with respect to receiver  $R_1$  (corresponds to point  $A$  in Figure 1(a)), we get that

$$\alpha = \arccos\left(\frac{|\vec{v}_2|}{|\vec{v}_1|}\right) \quad (1)$$

where  $\alpha$  is the angle  $\angle R_1 T R_2$ . Given  $\alpha$ , it can be easily shown that  $R_1$ ,  $T$ , and  $R_2$  need to be on a circle with a radius of

$$r = \frac{l}{2 \sin(\alpha)} \quad (2)$$

where  $l$  is the physical distance separating receivers  $R_1$  and  $R_2$ . Hence, the location of  $T$  can be found by introducing a third receiver  $R_3$  and measuring the angles  $\alpha_1 = \angle R_1 T R_2$  and  $\alpha_2 = \angle R_1 T R_3$ .

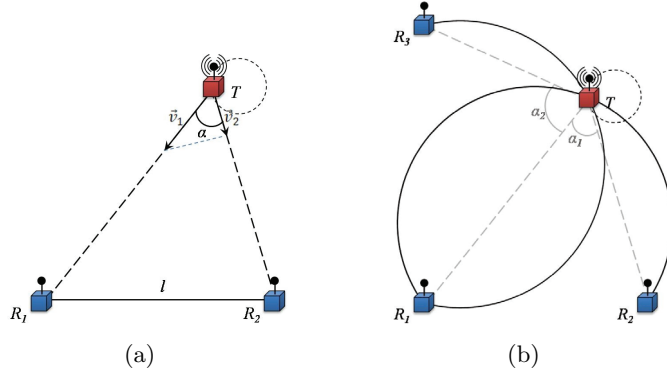


**Figure 2. Range estimation from  $\alpha$  angles**

While attractive, this method relies on measuring the Doppler shift at any one receiver accurately. However, in most computers and wireless devices, uncompensated crystal oscillators are used to generate the clock signals. The short-term stability of these oscillators are typically between  $10^{-8}$  and  $10^{-9}$  for one second. In our case, this corresponds to possibly more than 1 Hz error, because we cannot measure the baseline frequency directly (i.e. when the transmitter is stationary). We need to rely on measuring the difference between the maximum and the minimum frequencies and take their mean. Since the time between these events may not be much less than one second, short term stability can cause a larger error than the phenomenon we are trying to measure. Temperature-compensated crystal oscillators have somewhat better stability, while oven-controlled crystal oscillators are at least an order of magnitude more precise. Unfortunately, their price and power requirements are both significantly higher, and they are not used in everyday devices. The question is then how can we eliminate this significant source of error?

Notice that the transmit frequency instability has the same effect at both receivers because we compare their measurements at the same time. Hence, if we take the difference of the two measured frequencies, the actual transmit frequency is eliminated. This frequency difference relates to the difference of the observed speeds; however, not having the speed measurements available directly, only their difference, makes solving for the location somewhat more complicated. Given receivers  $R_1$  and  $R_2$ , we write the observed Doppler shifted frequencies for each receiver at time  $t$  as

$$f_{R_1}(t) = f_T \left( \frac{c}{c + |\vec{v}_{R_1}(t)|} - 1 \right), \quad f_{R_2}(t) = f_T \left( \frac{c}{c + |\vec{v}_{R_2}(t)|} - 1 \right), \quad (3)$$

where positive relative velocities correspond to a redshift in the observed frequencies. If we assume  $c \gg |\vec{v}(t)|$  and write the measured frequency difference as  $\Delta f(t) = f_{R_1}(t) - f_{R_2}(t)$ , substituting from equation (3) and simplifying gives

$$\Delta f(t) = -\frac{f_T}{c} (|\vec{v}_{R_1}(t)| - |\vec{v}_{R_2}(t)|), \quad (4)$$

and we now write

$$\Delta v(t) = |\vec{v}_{R_1}(t)| - |\vec{v}_{R_2}(t)| \quad (5)$$

Given  $\vec{v}(t)$  as the instantaneous velocity vector of  $T$  that is tangent to the circle of rotation, from Figure 3 we see  $|\vec{v}_{R_1}(t)| = |\vec{v}(t)| \cos(\beta(t))$  and  $|\vec{v}_{R_2}(t)| = |\vec{v}(t)| \cos(\gamma(t))$  as the projections of the velocity vector of the rotating transmitter onto the relative velocity vector of each receiver.

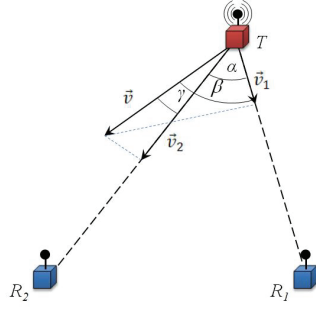


**Figure 3. Computation of angles**

To simplify further computation, we assume that the radius of the circle is infinitesimally small, that is, the velocity vector of the transmitter is rotating around one point. If the radius of the circle is small compared to the distance between the transmitter and the receiver, the error this assumption introduces is minimal. With this assumption, the angle  $\angle R_1 T R_2$ , denoted as  $\alpha$ , is fixed; therefore, we observe  $\beta(t) = \beta_0 + \phi(t)$ ,  $\gamma(t) = \gamma_0 + \phi(t)$ , and  $\gamma(t) = \beta(t) - \alpha$ . Substituting these relationships into equation (5) yields

$$\Delta v(t) = |\vec{v}(t)| (\cos(\beta_0 + \phi(t)) - \cos(\beta_0 + \phi(t) - \alpha)) \quad (6)$$

which can be rewritten as

$$\Delta v(t) = -2|\vec{v}(t)| \sin\left(\frac{2\beta_0 + 2\phi(t) - \alpha}{2}\right) \sin\left(\frac{\alpha}{2}\right) \quad (7)$$

Since  $\alpha$  is assumed to be constant, the maximum of  $\Delta v(t)$

$$\max(\Delta v(t)) = 2r\omega \sin\left(\frac{\alpha}{2}\right) \quad (8)$$

From here,  $\alpha$  can be computed as follows:

$$\alpha = 2 \arcsin\left(\frac{\max(\Delta v(t))}{2r\omega}\right) \quad (9)$$

In the presence of noise, however, the maximum of the signal cannot be measured precisely. To tackle this issue, we measure the power of the signal instead, because it is more resilient to noise due to the integration:

$$\alpha = 2 \arcsin\left(\frac{\sqrt{2}}{2r\omega} \sqrt{\int_0^{\frac{2\pi}{\omega}} \Delta v^2(t) dt}\right) \quad (10)$$

Performing this operation for each pair of receivers from the set of  $R_1$ ,  $R_2$ , and  $R_3$ , three distinct angles will be obtained ( $\alpha_1:(R_1, R_2)$ ,  $\alpha_2:(R_2, R_3)$ ,  $\alpha_3:(R_3, R_1)$ ). As described previously, each angle and the known positions of its corresponding receivers define a circle (see equation (2) and Figure 2(b)). Calculating the center of this circle and its radius for each estimate is straightforward and necessary for the localization estimate; however, this task is complicated by the symmetrical properties of the geometry. Each angle and its receivers define not one but two circles that are symmetrical about the chord between the positions of the receivers, i.e. the centers of the circles are reflections about a line connecting the locations of the two receivers. Resolving this dual solution would be impossible without knowing the direction of rotation of the transmitter  $T$ . While omitting details, we indicate here that assuming a known direction of rotation, the proper circle can be easily selected from the angular separation in time of the observed Doppler shifted frequencies between two receivers and their spatial relationship with the calculated centers of the symmetrical circles of interest. More plainly, each solution (circle), provided the assumed direction of rotation, will influence the order in which the two receivers observe their maximum/minimum Doppler shifted frequencies (e.g. either  $R_1$  before  $R_2$  or vice versa).

Accordingly, three unique circles are obtained (one for each  $\alpha$ ), and the desired localization estimate is calculated from their intersection points. Note, we obtain not one intersection point but up to three; therefore, the localization estimate is formulated as the geometric mean (centroid) of these points. Multiple points can be obtained since each pair of circles from the set of circles share a common intersection point at one of the receiver locations. For example, the circles for  $\alpha_1$  and  $\alpha_2$  are both defined by the receiver  $R_2$ ; therefore, these two circles intersect at the location of  $R_2$  and a second point. It is this second intersection point that should be near the location of transmitter  $T$  (assuming correct  $\alpha$  values). This point and the corresponding points for the two other combinations of circles form the input data of the centroid calculation.

### 3: Frequency Estimation

Accurate, continuous frequency estimation is one of the key requirements for the proposed localization method. Moreover, multiple receivers are required to measure the envelope frequency in a synchronized manner with minimal communication and scheduling overhead for the approach to scale well. The accuracy requirements and the need for experimenting with new synchronization and estimation methods suggested a more powerful and more flexible platform than those used previously in radio interferometric localization [10] [8]. Software Defined Radio (SDR) is a promising approach not only for increasing the computational budget, but also for making detailed observations on the signals. We selected the GNU Radio [6] software platform and the USRP [5] hardware frontend to verify the proposed ranging ideas.

The baseline configuration consists of a fixed position SDR transmitter and a rotating transmitter. The rotating node emits a pure sine wave continuously, thus it can be implemented using a simple, low-cost device, such as a wireless sensor node. The second, fixed position transmitter transmits a pure sine wave at a close frequency. Since multiple receivers need to make synchronized measurements, a time synchronization approach is necessary. Instead of implementing a time synchronization protocol on the SDR platform, we embed timing information in the transmitted signal itself. The SDR transmitter peri-

odically emits a windowed chirp signal before a pure sine wave segment. That chirp can be accurately decoded on the receiver side and it makes a common time reference point for all receivers. The range of this short frequency sweep does not overlap with the frequencies of the pure sinusoids.

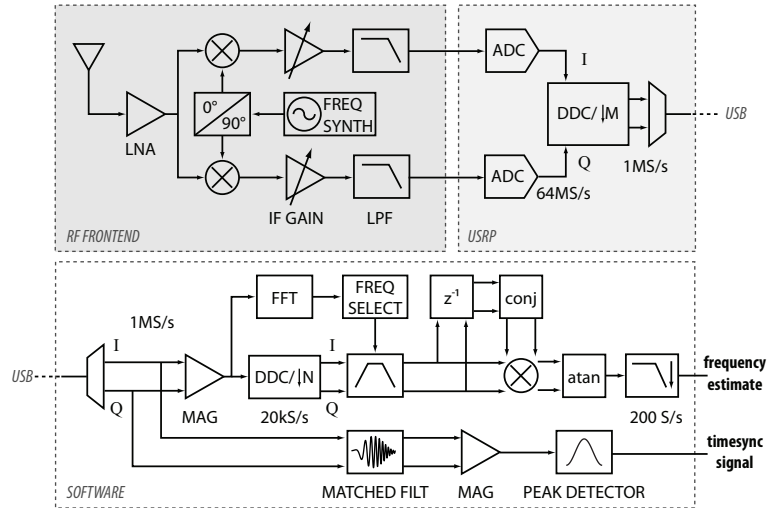


**Figure 4. Signal flow diagram of the receiver node**

The architecture of a receiver node is shown in Figure 4. The top part of the diagram demonstrates the signal flow in the RF frontend and the USRP digital frontend. The selected RF module can be tuned in the 400-500 MHz range by controlling the on-board PLL. The downconverted and amplified (0-60dB) complex analog signal is digitized by the USRP motherboard at a fixed rate and resolution (64 MS/s, 12 bit). Due to the bandwidth limitation on the USB bus and the coarse-grained tuning steps of the analog mixer, the FPGA in the digital frontend implements a digital downconversion step before sending the samples to the PC. In the current application, the USB stream is a 1 MS/s complex signal (1 MHz IF bandwidth), and the carriers are around 100 kHz with a few hundred Hz separation. In the IF stage, the chirp signal sweeps from DC to 10 kHz.

The lower part of Figure 4 describes the signal processing steps on the software side. On the GNU Radio platform, the signal processing blocks are implemented in C++, but the blocks are configured and wired by Python scripts, which provides a very flexible environment without compromising performance. Although many of the signal processing steps of the proposed approach (envelope decoding, time synchronization, filtering) are implemented on the GNU Radio platform, the published results are based on recorded data and offline processing in MATLAB [1]. However, the final signal processing chain contains no steps which are infeasible to implement in a real-time GNU Radio application.

The time synchronization decoder processes the received samples independently from the rest of the signal processing path and produces time reference points at the end of the chain. It uses a matched filter and a peak detector to find the exact position of the chirp signal in the data stream. The current implementation provides 1  $\mu$ s accuracy which is far better than required here.

Figure 5 shows the results at key intermediate steps along the main signal processing path. These signals were captured in a stationary setup (both transmitters—one SDR

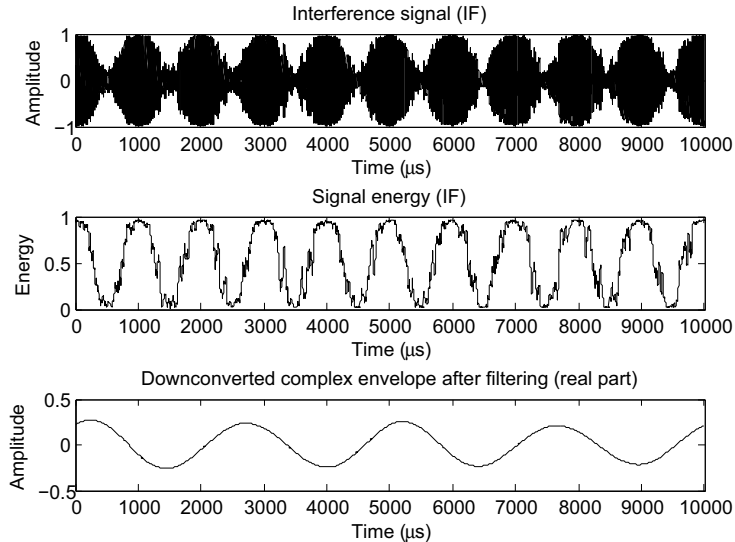


**Figure 5. Captured and processed interference signal**

node and one XSM mote [4]—were fixed) to measure the accuracy and repeatability of the proposed approach. At the first stage of the chain, the complex samples are used to calculate the instantaneous signal energy (squared envelope signal). This signal (second in Figure 5) is very noisy and usually has a significant DC component. Also, it has non-complex samples but a higher than necessary sampling frequency. Thus, before filtering, it goes through a complex digital downconversion step. The next step is essential: it employs a very narrow bandpass filter to remove most of the noise, the DC component, and the images introduced by the digital mixer. The bandpass filter (6th order elliptic IIR) is run-time tuned by a coarse grained FFT-based frequency estimator. The final result of the frequency estimator (real part) is shown on the third line of Figure 5. Note, the frequency of this signal significantly differs from the original envelope frequency due to the digital downconversion step. The main role of the digital downconverter (DDC) block is to “reconstruct” the complex sample pairs, so one can consider this as a side effect in this application. Since we are interested only in the frequency fluctuation of the signal, this constant shift is irrelevant for ranging purposes. However, the frequency of the digital mixer has to be selected carefully since the unfiltered signal contains many frequency components that might get converted or aliased to near the envelope frequency. Currently, the DDC uses  $\frac{3}{5}$  of the envelope frequency estimated by the FFT. The complex pairs are processed by a simple FM demodulator which quickly provides an estimate of the instantaneous frequency. Finally, the frequency output is low-pass filtered and decimated.

## 4: Results

In this section, we present experimental results and characterize the corresponding measurement noise. We also provide simulation results for localization accuracy and evaluate the location solver’s sensitivity to measurement errors.

## 4.1: Experimental Results

Figure 6 shows the frequency estimation results using a stationary setup: one XSM transmitter, one SDR transmitter and two SDR receivers. Since none of the transmitters is moving, the frequency plots should show a straight horizontal line. However, the results clearly indicate a significant change (3 Hz) in the envelope frequency even during this short time interval (700 ms). This drift is due to the instability of the transmitters' oscillators, and it is measured by the two independent receivers consistently. The right side of Figure 6 gives a clearer picture of the accuracy of the frequency estimation method by showing the difference between the two frequency plots. Ideally, the difference should be zero in this stationary setup. In this particular experiment, it fluctuates between  $\pm 0.1$  Hz. In case of a rotating transmitter, the bandwidth of the signal is determined by the speed and radius of rotation. It is typically a few Hz; hence, the output of the frequency estimator could be smoothed by a low-pass filter to increase the SNR.

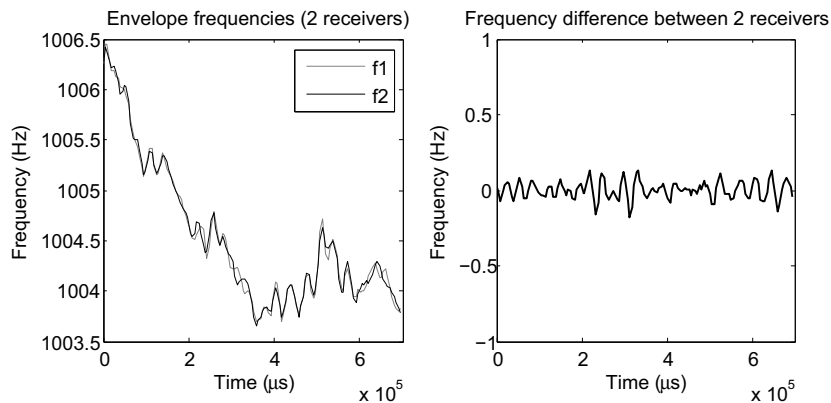


**Figure 6. Frequency estimation results**

In a slightly modified configuration, we used two fixed position SDR transmitters and two SDR receivers indoors and executed 300 experiments—one every 10 seconds—as previously described. A single experiment resulted in 100 frequency estimates. During the full set of experiments (50 min, 300,000 estimates), the largest difference of the measured envelope frequency was 63.8 Hz, again due to the instability of the transmit frequency. However, the two receivers never differed by more than 0.5 Hz (maximum error) and the standard deviation of their difference was 0.045 Hz.

The central component of the signal processing chain is the frequency estimator for which many different methods have been developed and published [10][12]. We selected, implemented, and evaluated some of these, but one of the potential future directions is a more exhaustive study and analysis of the applicability of existing methods.

## 4.2: Simulation Results

The simulator generates Doppler shifted envelope frequencies at each receiver over a time interval. The signal is calculated from the known geometry of the nodes and the configuration parameters, such as rotation radius, speed, etc. The simulator also adds noise to the generated signals (zero-mean Gaussian noise with adjustable standard deviation).

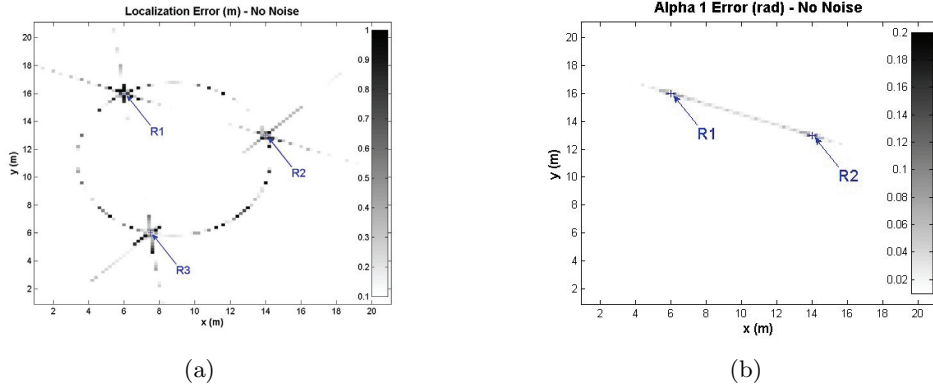


**Figure 7. Simulation results with no noise**

Each localization estimate is then formulated according to the steps detailed in Section 2. From an input data set of Doppler shifted frequency measurements, the velocity differences between each pairwise combination of receivers (see equations (3 - 5)) are used to calculate the  $\alpha$  angles according to the relationship in equation (10). From each calculated  $\alpha$ , the corresponding circles are calculated (see Figure 2(b)), and the centroid of their pairwise intersection points forms the localization estimate.

For the following experiments, we assume three static receivers  $R_1$ ,  $R_2$ , and  $R_3$  positioned at locations (6, 16), (14, 13), and (7.5, 6) meters, respectively. The fixed transmission frequencies of the two transmitters  $T'$  and  $T$  are 430 MHz and 431 MHz ( $\delta f = 1$  kHz), respectively. Regarding the rotating transmitter  $T$ , the radius of rotation is 0.12 m, the rate is 45 RPM ( $\omega = 4.71$  rad/s), and the direction is counterclockwise. Assuming the speed of light is  $3.0 \times 10^8$  m/s, using equation (3) and the relationship  $|\vec{v}(t)| = r\omega$  yields an expected Doppler shift ranging between  $\pm 0.81$  Hz.

The simulation was conducted by sweeping the location of  $T$  between 1 to 21 meters along both the x and y axes in 0.2 m increments. Simulation results for locations where any receiver is within the circle of rotation of the rotating transmitter  $T$  are ignored.

Figure 7 shows the simulation results for the experiment with no noise present in the generated input data. Figure 7(a) is an error plot of the localization estimate over all of the simulated positions of transmitter  $T$ . The calculated error is the magnitude of the distance between the known position of  $T$  and the estimated position. The colorbar on the right-hand side shows the color distribution over a range of errors where the units are in meters (localization errors below 0.1 m are white and above 1.0 m are black). The maximum obtained error was 5.5 m which occurred when  $T$  was at location (5.8, 16.2), i.e. directly adjacent to  $R_1$ . We see from Figure 7(a) that almost all significant points of error occur when  $T$  lies directly on the lines connecting any two receivers and on the circle defined by the locations of the three receivers. This is intuitive since the former implies at least one calculated  $\alpha$  angle that is very near  $\pi$  radians. Such an angle measure results in a very large circle defined by the method of Figure 2(b), which is very susceptible to errors. The latter errors are present since the calculated circles from Figure 2(b) will overlap, i.e. a lack of distinct intersection points invalidates the centroid calculation.

Figure 7(b) shows the same type of error plot for the calculated angle  $\alpha_1$  ( $\alpha$  angle between receivers  $R_1$  and  $R_2$ ). The colorbar (in units of radians) indicates calculated  $\alpha_1$ 's with errors below 0.01 radians are white and above 0.2 radians are black. From the plot

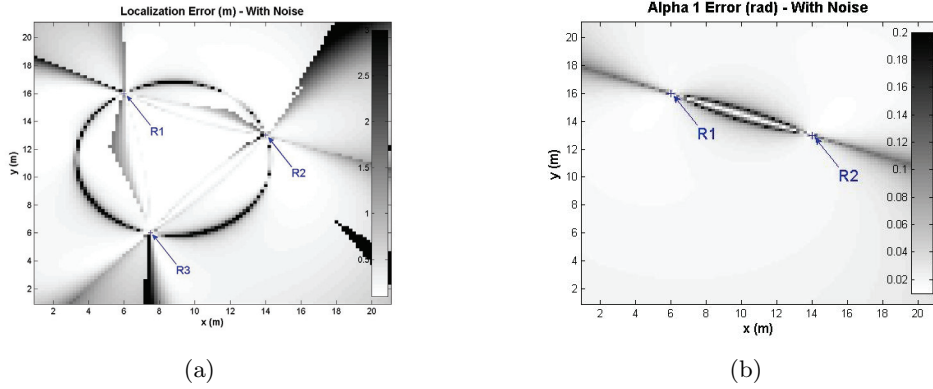


**Figure 8. Simulation results with noise**

we see that the only significant errors occur when  $T$  is positioned on the line connecting receivers  $R_1$  and  $R_2$ . The presence of the errors can be attributed to the assumption that the  $\alpha$ 's are constant while the transmitter is rotating. It follows from our approximation that the radius of rotation is negligible.

The same experiment was conducted with zero-mean Gaussian noise added to the generated frequency measurement signals of each of the receivers. The standard deviation of the added noise was set to 6.0% of the maximum expected Doppler shift. This was determined based on the error characteristics of the experimentally gathered data. Figure 8 shows the simulation results for this experiment. Notice that the colorbar of Figure 8(a) has been adjusted to have a new upper limit of 3.0 m in order to show the error distribution. The maximum obtained error was 11.69 m which occurred when  $T$  was at location (21, 12). We see from Figure 8(a) that the majority of the significant errors still occur when  $T$  lies directly on the lines connecting any two receivers and on the circle defined by the locations of the three receivers; however, as expected, a larger distribution of errors is present with gradual degradations in accuracy where the degenerate geometries exist. Note that inside the triangle formed by the three receivers, other than close to the edges of the triangle, the error is uniformly below 0.1 m. As can be seen in the figure, significant areas outside the triangle have low error also. Adding a fourth receiver could eliminate the "blind spots" of our method by placing them in such a way that any point can be localized accurately using three out of the four receivers. A simple outlier rejection approach could be used to identify the receiver that is in a bad position with respect to the transmitter. However, we leave this to future work.

Figure 8(b) shows the error plot for the calculated angle  $\alpha_1$  with the noisy input data. The colorbar distribution is the same as the previous experiment ( $\alpha_1$ 's with errors below 0.01 radians are white and above 0.2 radians are black). We observe the errors along the line connecting the receivers are accentuated. Note the interesting error pattern along the line in between the receivers; the largest errors along the line occur at a distance of about one radius ( $r$  of  $T$ ) off the line. This phenomenon can most likely be attributed to the influence of the noise on the  $\alpha$  calculations in conjunction with the zero-radius approximation inherent in our method.

## 5: Conclusion

We presented a novel idea for ranging and localization of wireless radio nodes and our preliminary work validating it. While we have not carried out measurements with an actual rotating transmitter, the stationery experiments and simulation results indicate that the method is not only feasible, but has the potential for achieving high-accuracy localization. In fact, we have barely scratched the surface of what's possible. We have not explored different cases, for example, where the rotating transmitter is at a known position and the tracked node is a receiver. We have not assumed that the rotating node can be synchronized to the receivers, which would provide bearing information. If the transmit frequency is stable in the short term (using, for example, an oven-controlled oscillator), then measuring the maximum of the Doppler shift provides 3D bearing, since the maximum observable speed in the plane of the rotation is given by the known radius and angular rate.

## References

- [1] Mathworks Simulink/Stateflow Tools. <http://www.mathworks.com>.
- [2] P. Bahl and V. N. Padmanabhan. Radar: An in-building RF-based user-location and tracking system. *Proc. IEEE INFOCOM*, 2:77584, March 2000.
- [3] Chipcon AS, CC1000: Single chip very low power RF transceiver. <http://www.chipcon.com>, 2004.
- [4] P. Dutta, M. Grimmer, A. Arora, S. Bibyk, and D. Culler. Design of a wireless sensor network platform for detecting rare, random, and ephemeral events. *In Proc. of IPSN/SPOTS*, 2005.
- [5] Ettus Research LLC. <http://www.ettus.com/>.
- [6] GNU Radio website. <http://gnuradio.org/>.
- [7] A. Harter, A. Hopper, P. Stegglesand, A. Ward, and P. Webster. The anatomy of a context-aware application. *In Mobile Computing and Networking*, page 5968, 1999.
- [8] B. Kusý, G. Balogh, Á. Lédeczi, J. Sallai, and M. Maróti. inTrack: High precision tracking of mobile sensor nodes. *In Proc. of EWSN*, January 2007.
- [9] B. Kusy, A. Ledeczi, and X. Koutsoukos. Tracking mobile nodes using rf doppler shifts. *In Proc. of ACM SenSys*, 2007.
- [10] M. Maróti, B. Kusý, G. Balogh, P. Völgyesi, A. Nádas, K. Molnár, S. Dóra, and Á. Lédeczi. Radio interferometric geolocation. *In Proc. of ACM SenSys*, November 2005.
- [11] PanGo. <http://www.pangonetworks.com>.
- [12] B. G. Quinn and E. J. Hannan. *The Estimation and Tracking of Frequency*. Cambridge University Press, 2001.
- [13] D. Taubenheim, S. Kyperountas, and N. Correal. Distributed radiolocation hardware core for ieee 802.15.4. Technical report, Motorola Labs, Plantation, Florida, 2005.
- [14] R. Want, A. Hopper, V. Falcao, and J. Gibbons. The active badge location system. *ACM Transactions on Information Systems*, 40, 1992.
- [15] M. Youssef and A. Agrawala. The horus wlan location determination system. *In Proc. MobiSys*, 2005.